Research Article | Vol. 28, No. 26 / 21 December 2020 / Optics Express 39453

Optics EXPRESS

Polarization-differentiated band dynamics of resonant leaky modes at the lattice Γ point

Sun-Goo Lee,[1] Seong-Han Kim,[1] Chul-Sik Kee,[1] and Robert Magnusson[2,*]

[1] *Integrated Optics Laboratory, Advanced Photonics Research Institute, Gwangju Institute of Science and Technology, Gwangju 61005, Republic of Korea*
[2] *Department of Electrical Engineering, University of Texas at Arlington, Arlington, Texas 76019, USA*
[*] *magnusson@uta.edu*

Abstract: In the physical description of photonic lattices, leaky-mode resonance and bound states in the continuum are central concepts. Understanding of their existence conditions and dependence on lattice parameters is of fundamental interest. Primary leaky-wave effects are associated with the second stop band at the photonic lattice Γ point. The pertinent band gap is defined by the frequency difference between the leaky-mode band edge and the bound-state edge. This paper address the polarization properties of the band gaps resident in laterally periodic one-dimensional photonic lattices. We show that the band gaps pertinent to TM and TE leaky modes exhibit significantly differentiated evolution as the lattice parameters vary. This is because the TM band gap is governed by a surface effect due to the discontinuity of the dielectric constant at the interfaces of the photonic lattice as well as by a Bragg effect due to the periodic in-plane dielectric constant modulation. We find that when the lattice is thin (thick), the surface (Bragg) effect dominates the Bragg (surface) effect in the formation of the TM band. This leads to complex TM band dynamics with multiple band closures possible under parametric variation. In complete contrast, the TE band gap is governed only by the Bragg effect thus exhibiting simpler band dynamics. This research elucidates the important effect of polarization on resonant leaky-mode band dynamics whose explanation has heretofore not been available.

1. Introduction

In photonic lattices with thin-film geometry, guided electromagnetic waves are classified according to polarization state. A transverse electric (TE) mode is characterized by an electric field vector being parallel to the film surface and a transverse magnetic (TM) mode by a magnetic field vector similarly oriented. It is well-known that photonic band gaps are opened by Bragg effects due to the periodic modulation of the dielectric function in photonic lattices [1,2]. Recently, however, it has been reported that first-order TM band gaps are governed by not only the Bragg effect but also the discontinuity of the dielectric constant at the film surfaces, while TE band gaps formed only by the Bragg effect [3,4]. Hence the band gaps induced by TE and TM modes exhibit different evolution as the film thickness varies. As a result of the interplay between the two distinct mechanisms, the first-order TM band gaps exhibit band gap closure and band flip phenomena wherein modal profiles of band-edge modes are reversed. The first-order (non-leaky only) TE band gap, induced solely by the Bragg effect, does not show band closure and band flips [4].

Guided waves in one-dimensional (1D) and 2D thin-film photonic lattices have been utilized widely to manipulate light propagation and localization at subwavelength scales. Especially, leaky and nonleaky lateral Bloch modes at the second stop bands that open at the second-order Γ point, are of interest. Leaky band edge modes generate diverse spectral responses via resonant coupling with normally incident waves [5–12] and nonleaky edge modes become bound states in the continuum (BICs) currently of great scientific interest [13–28]. Recent studies on the band

#413357 https://doi.org/10.1364/OE.413357
Journal © 2020 Received 27 Oct 2020; revised 20 Nov 2020; accepted 20 Nov 2020; published 14 Dec 2020

Optics EXPRESS

dynamics of 1D photonic lattices have shown that the second TE band gap is primarily formed by interplay between two Bragg processes due to the first and second Fourier harmonic of dielectric constant modulation [29,30]. Destructive interference of the two distinct Bragg effects closes the second TE band and induces a band flip and inter-band bound state transition whereby the leaky edge and BIC edge transit across the band gap. Before and after band gap closure, TE-polarized symmetry-protected BICs locate below and above the leaky edges.

Symmetric photonic lattices, that possess time reversal and inversion symmetry, support both TE- and TM-polarized BICs at the nonleaky edges of the second TE and TM stop bands, respectively. Since only TM modes are affected by the discontinuity of dielectric constant at the interfaces of thin-films, different band dynamics, including band gap closure, band flip, and bound-state transition, are expected for TE and TM band gaps. In this paper, we investigate the band dynamics of TM- and TE-polarized leaky modes at the second-order Γ point, and clarify the fundamentally different aspects between the second TE and TM band gaps in a representative 1D photonic lattice. Whereas analogous study has been conducted for thin-film lattices under first Bragg scattering [4], this has not been done for the leaky-mode case. The physics and formulation of these cases differ significantly.

2. Lattice structure and perspective

Figure 1 illustrates our simple model, the coupling processes at the second leaky stop band, and the attendant photonic band structures indicating inter-band bound-state transitions. As shown in Fig. 1(a), we analyze a single 1D periodic lattice of thickness d composed of alternating media with high (ϵ_h) and low (ϵ_l) dielectric constants and surrounded by a background medium of ϵ_s. The width of the high and low dielectric part is $\rho\Lambda$ and $(1-\rho)\Lambda$, respectively, where Λ is the period. By means of the total internal reflection, this simple lattice supports both TE- and TM-polarized guided modes because its average dielectric constant for TE mode, $\epsilon_{\mathrm{TE}} = \epsilon_l + \rho(\epsilon_h - \epsilon_l)$, and for TM mode, $\epsilon_{\mathrm{TM}} = [\rho/\epsilon_h + (1-\rho)/\epsilon_l]^{-1}$, is larger than $\epsilon_s = 1$. With the periodic dielectric constant modulation, guided modes are described by the complex frequency $\Omega = \Omega_{\mathrm{Re}} + i\Omega_{\mathrm{Im}}$, where the imaginary part Ω_{Im} is associated with radiative loss.

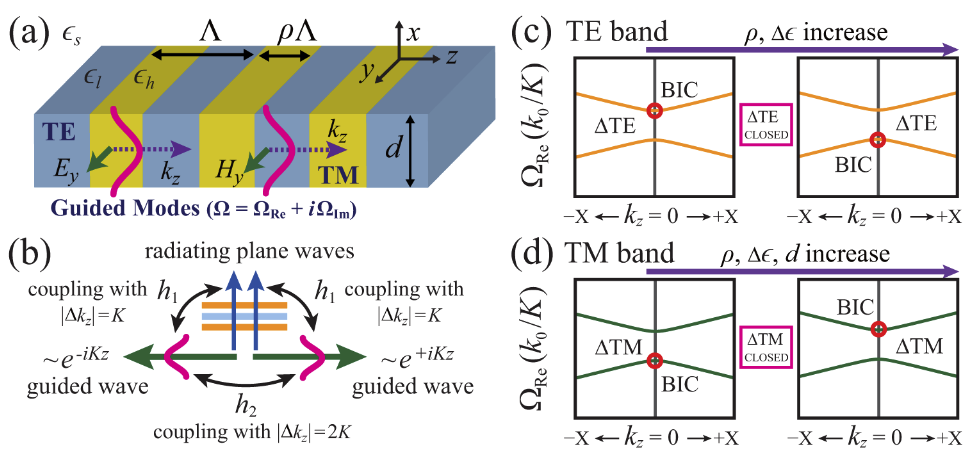

Fig. 1. (a) Schematic of a 1D photonic lattice for studying band dynamics of TM- and TE-polarized leaky modes. Guided modes are described by complex frequency $\Omega = \Omega_{\mathrm{Re}} + i\Omega_{\mathrm{Im}}$. (b) Coupling processes induce the second leaky band gap. Conceptual illustration of the band transition of (c) TE- and (d) TM-polarized BICs. The size of the TE and TM band gaps varies by lattice parameters. Before and after the band gap closure, the spectral locations of the BIC edges and leaky edges are reversed.

In this simple case, TE and TM band gaps are opened by the scattering processes due to the periodic dielectric constant modulation when $\Delta\epsilon = \epsilon_h - \epsilon_l > 0$ and $0 < \rho < 1$. Figure 1(b) conceptually illustrates the coupling processes inducing the second leaky stop band of interest in this study. In Fig. 1, h_1 and h_2 represent the coupling coefficients associated with the first and second Fourier harmonic of the spatial dielectric constant modulation, respectively [31,32]. The second stop band is opened primarily by the second Fourier harmonic (h_2) and secondarily by the first Fourier harmonic (h_1). Near the second stop band, the quasi-guided modes lose their electromagnetic energy as time goes on due to the phase-matched coupling process (h_1) with the outside plane wave. In the symmetric lattice with $\epsilon(x, z) = \epsilon^*(x, -z)$ shown in Fig. 1(a), however, one of the edge modes suffers no radiation loss and becomes a symmetry-protected BIC at the second TE and TM band gaps.

The size of the second TE band gap is determined primarily by the parameters $\Delta\epsilon$ and ρ. As schematically illustrated in Fig. 1(c), the TE band gap, ΔTE, is opened at $k_z = 0$, and a symmetry-protected BIC in a red circle appears at the upper band edge when $\Delta\epsilon$ and ρ are small. With proper values of $\Delta\epsilon$ and ρ, the TE band gap closes and the two band edge modes are degenerated. The spectral location of the TE-polarized BIC transits from the upper to the lower band edge as the values of $\Delta\epsilon$ and/or ρ increase. We note that the second TE band gap can be closed only when ρ is less than 0.5. For the fixed value of $\Delta\epsilon$ ($\rho<0.5$), there exists only one value of $\rho<0.5$ ($\Delta\epsilon$) where the TE band closes. As illustrated schematically in Fig. 1(d), unlike the TE band, d as well as $\Delta\epsilon$ and ρ considerably contribute to close the second TM band gap, ΔTM. The spectral location of the TM-polarized BIC changes also by the variation of $\Delta\epsilon$, ρ, and d. In this study, we investigate the band dynamics of TM- and TE-polarized leaky modes through rigorous finite-element method (FEM) simulations and a semianalytical dispersion model, and thereby elucidate the essential properties of, and differences between, the TM and TE stop bands. This is the major contribution of the research presented here.

3. Leaky-mode band dynamics

As shown in Fig. 2(a), the second TM and TE stop bands open at the second-order Γ point due to the periodic modulations in dielectric constant. The TM band gap locates above the TE gap because the effective index of the TM mode is lower than that of the TE mode, as usual. This agrees with previous experimental results [11,12]. Simulated spatial magnetic (electric) field, H_y (E_y), distributions for TM (TE) mode in the insets indicate that the upper (lower) band edge mode with symmetric field distributions is radiative out of the grating layer, while the lower (upper) band edge mode with asymmetric field distributions is well localized in the lattice. The existence of symmetry-protected BIC at the second TM and TE band gaps can be confirmed by investigating the radiative Q factors illustrated in Fig. 2(b). At the TM (TE) band gap, the symmetry-protected BIC in the lower (upper) band edge exhibits a Q factor that is larger than 10^{14} at $k_z = 0$, but the Q values decrease abruptly as k_z drifts from the Γ point. As depicted in Fig. 2(c), at normal incidence with $\theta = 0°$, only one resonance appears in the transmission curve due to the leaky mode in the upper (lower) edge of the TM (TE) stop band. The symmetry-protected BIC in the lower (upper) edge of the TM (TE) stop band is not seen in the transmission curve. When $\theta = 5°$, on the other hand, with the symmetry broken, two guided-mode resonances due to the leaky Bloch modes in the upper and lower bands appear in the transmission curve, simultaneously. The location of the resonance follows the phase matching condition $k_0 \sin\theta = k_z$. Since the second TE and TM band gaps locate in the subwavelength region ($\lambda > \Lambda$), transmission curves in Fig. 2(c) reflect only highly efficient zero-order diffraction effects. In Fig. 2(c), the normalized frequency scale is from 0.35 to 0.41 for TE mode. If we set $\Lambda = 1$ µm, this gives a wavelength range from 2.44 µm to 2.86 µm.

FEM simulated results illustrated in Figs. 2(a)–2(c) clearly show that both the second TM and TE band gaps admit a leaky edge and a BIC edge, simultaneously. External waves incident

Optics EXPRESS

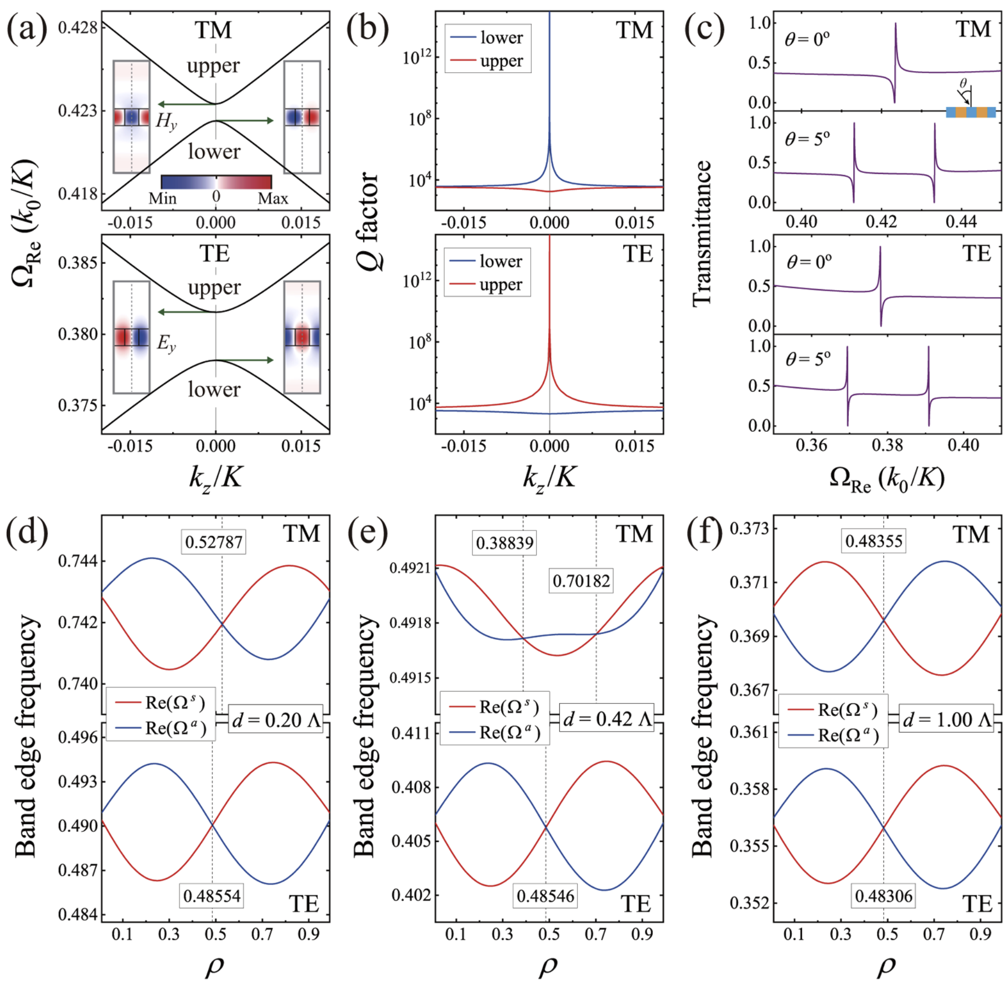

Fig. 2. Comparison between the key properties of the second TM stop band and those of the second TE band. (a) Dispersion relations, (b) radiative Q factors, (c) transmission spectra. Spatial magnetic and electric field distributions in the insets in Fig. 2(a) indicate that one of the band edge modes becomes the nonleaky symmetry-protected BICs. Evolutions of the band edge frequencies as a function of ρ when (d) $d = 0.20\ \Lambda$, (e) $d = 0.42\ \Lambda$, and (f) $d = 1.00\ \Lambda$. As ρ varies from 0 to 1, TM and TE band gaps exhibit closed band states where the upper and lower band edges are degenerate. Before and after the band gap closure, the spectral locations of BIC edges and leaky edges are reversed. In the FEM simulations, parameters $\Delta\epsilon = 1.00$ and $\epsilon_{\rm TM} = \epsilon_{\rm TE} = 9.00$ are kept constant, and we use $d = 0.60\ \Lambda$ and $\rho = 0.40$ for (a), (b), and (c).

on a periodic lattice couple to the phased-matched TM- or TE-polarized leaky modes and generate guided-mode resonance effects in the transmission curve. However, relative positions of the leaky edge and the BIC edge are different. Noticeable difference between the second TM and TE band gap can be seen by comparing the evolution of the band edge frequencies as a function of ρ. Figure 2(d) with thickness $d = 0.20\ \Lambda$ indicates that as ρ increases from zero, the TM (TE) band gap opens and its size increases, decreases, and becomes zero when $\rho = 0.52787$ ($\rho = 0.48554$). The second TM (TE) band gap reopens and its size increases, decreases, and approaches zero when ρ is further increased and approaches 1. When $d = 0.20\ \Lambda$, there is a closed band state, and before and after the band gap closure, the symmetry-protected TM-polarized (TE-polarized) BICs are located at the upper and lower edges of the TM (TE) band gaps, respectively. When $d = 0.42\ \Lambda$, as shown in Fig. 2(e), the TM band exhibits closed band states two times at $\rho = 0.38839$ and 0.70282, while the TE band shows a closed band state at $\rho = 0.48546$ as ρ varies from 0 to 1. When $d = 1.00\ \Lambda$, as shown in Fig. 2(f), both the TM and TE bands exhibit a closed band state at $\rho = 0.48355$ and 0.48306, respectively. But before and after the band gap closure, TM-polarized (TE-polarized) BICs are located at the lower (upper) and upper (lower) edges of the TM (TE) band gaps, respectively.

To summarize the evolutions of the band-edge frequencies plotted in Figs. 2(d)–2(f), the spectral location of the TE-polarized BIC transfers from the upper to lower band edge by passing through the degenerate point as ρ varies from 0 to 1, irrespective of d. The critical value of the fill factor where the TE band gap closes is less than 0.5 irrespective of d. Simulated critical value of ρ as a function of thickness d, shown in Fig. 3(a), reveals that for TE mode, the variation of thickness barely affects the position of the critical value of ρ. In contrast, the spectral location of the TM-polarized BIC depends considerably on the thickness d as well as the fill factor ρ. Not only can the TM band be closed when $\rho>0.5$ or $\rho<0.5$ but also the number of closed-band states is affected by the thickness. Figure 3(b) illustrates the simulated critical values of ρ where the TM band gap closes. When $d<0.39\ \Lambda$ and $d>0.44\ \Lambda$, the TM band gap closes once near fill factor 0.5. When $0.39\ \Lambda \le d \le 0.44\ \Lambda$, in contrast, Fig. 3(b) shows that the TM band gap closes two times.

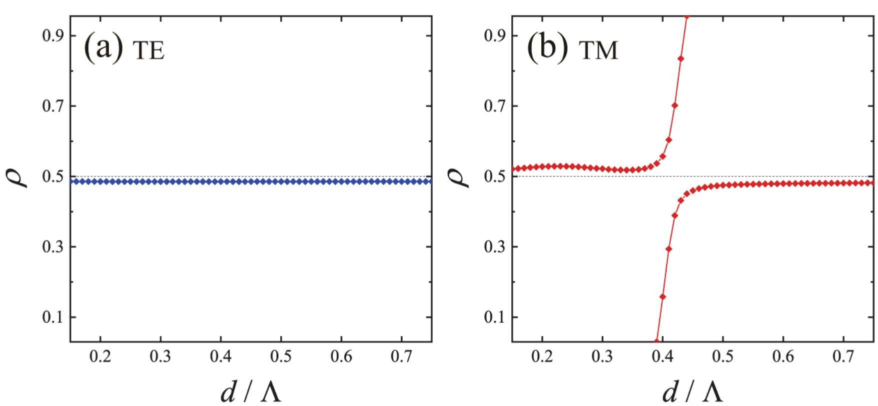

Fig. 3. FEM-simulated critical value of ρ where (a) TE and (b) TM band gap closes as a function of thickness d. Lattice parameters are the same as for Fig. 2. In the FEM simulations, d is increased in discrete steps of 0.01 Λ.

4. Coupled-mode analysis

To understand the different evolution of the second TM and TE band gaps illustrated in Fig. 2, we investigate the dispersion relations of TM-polarized guided waves by solving the 1D wave

Optics EXPRESS

equation given by [33]

$$\frac{\partial}{\partial x}\left(\xi\frac{\partial H_y}{\partial x}\right)+\frac{\partial}{\partial z}\left(\xi\frac{\partial H_y}{\partial z}\right)+k_0^2H_y=0, \tag{1}$$

where k_0 denotes the wave number in free space and $\xi = 1/\epsilon$ is the inverse of the dielectric function. Conventionally, Eq. (1) can be solved numerically by representing the magnetic field H_y as the sum of Bloch waves and by expanding the inverse of the dielectric function $\xi(x,z)$ in a Fourier series [34]. To obtain clear insight into the formation of the second TM band by the interplay between the first and second Fourier harmonics of the periodic dielectric function, in this study, we solve the wave equation by using a simple semianalytical dispersion model in which the spatial magnetic field distributions and the inverse of the dielectric functions are approximated as [31]

$$H_y(x,z)\approx(Ae^{+iKz}+Be^{-iKz})\varphi_{\mathrm{TM}}(x)+H_r, \tag{2}$$

$$\xi(x,z)\approx\xi_0(x)+\xi_1(x)\cos(Kz)+\xi_2(x)\cos(2Kz). \tag{3}$$

In Eq. (2), A and B are slowly varying envelopes of two counter-propagating waves, $\varphi_{\mathrm{TM}}(x)$ characterizes the transverse mode profile of the homogeneous slab waveguide with dielectric constant ϵ_0, and H_r represents the radiating diffracted wave. In Eq. (3), $\xi_0(x) = \rho/\epsilon_h + (1-\rho)/\epsilon_l$ and $\xi_{n=1,2}(x) = (-2\Delta\epsilon)/(n\pi\epsilon_h\epsilon_l)\times\sin(n\pi\rho)$ when $x\in[-d,0]$ and $\xi_0(x)=\epsilon_s$ and $\xi_{n=1,2}(x)=0$ when $x\notin[-d,0]$. We expect that the semianalytical approach is valid at and near the second stop band because the higher-order Fourier harmonics $\xi_{n\geq3}(x)\cos(nKz)$ cannot contribute to the second stop band. The dispersion model for studying the second TM band gap herein is modified from the Kazarinov and Henry (KH) model [31]; it has been verified by rigorous calculation in many cases that the KH dispersion model describes well the dynamics of the second TE band of weakly modulated photonic lattices [29,30]. Accordingly, the present extension to the TM case is well justified.

By solving the wave equation in Eq. (1) with the approximated spatial dielectric function and field distributions, dispersion relations near the second band edges can be written as

$$\Omega(k_z)=\Omega_0-\left(ih_1\pm\sqrt{k_z^2+(h_2+ih_1)^2}\right)/(Kh_0), \tag{4}$$

where h_0, h_1, and h_2 represent the coupling coefficient associated with the zeroth, first, and second Fourier harmonics, respectively, and Ω_0 is the Bragg frequency under vanishing index modulation ($\Delta\epsilon = 0$). We note that Eq. (4) is valid for both TE and TM modes with different coupling coefficients even though dispersion relations for TE mode are obtained from a different wave equation [29–32]. Coupling coefficients for TE mode were introduced in previous studies and in this study we present the coupling coefficients for TM modes as

$$h_{0,\mathrm{TM}}=\Omega\int_{-\infty}^{\infty}\varphi_{\mathrm{TM}}(x)\varphi^*_{\mathrm{TM}}(x)dx, \tag{5}$$

$$h_{1,\mathrm{TM}}=i\frac{\xi_1^2}{8\Omega^2K^3}\int_{-d}^{0}\int_{-d}^{0}\frac{d\varphi^*_{\mathrm{TM}}(x)}{dx}\frac{d\varphi_{\mathrm{TM}}(x')}{dx'}\frac{\partial^2G_{\mathrm{TM}}(x,x')}{\partial x\partial x'}dx'dx, \tag{6}$$

$$h_{2,\mathrm{TM}}=\frac{\xi_2}{4K}\int_{-d}^{0}\left(K^2\varphi_{\mathrm{TM}}(x)\varphi^*_{\mathrm{TM}}(x)-\frac{d\varphi_{\mathrm{TM}}(x)}{dx}\frac{d\varphi^*_{\mathrm{TM}}(x)}{dx}\right)dx, \tag{7}$$

where $G_{\mathrm{TM}}(x,x')$ denotes the Green's function for the diffracted field for TM modes.

As displayed in Eq. (4), the second TM band gap with two band-edge frequencies $\Omega^a = \Omega_0 + h_2/(Kh_0)$ and $\Omega^s = \Omega_0 - (h_2 + i2h_1)/(Kh_0)$ opens at $k_z = 0$. The two band edge modes are standing waves with zero group velocity formed by two counter-propagating waves, $A\exp(+iKz)$ and $B\exp(-iKz)$. One band edge mode with purely real frequency Ω^a, that is obtained when

Optics EXPRESS

the magnetic field distribution in Eq. (2) is an asymmetric sine function ($A = -B$), becomes a BIC because two radiating waves by $A\exp(+iKz)$ and $B\exp(-iKz)$ cancel each other out by total destructive interference. The band edge mode with Ω^a is called the symmetry-protected BIC because the vanishing radiation loss can be interpreted to be due to the symmetry mismatch between the asymmetric eigenmode of the photonic lattice and the outside plane wave in the radiation continuum. The other band edge mode with Ω^s, that is obtained when the magnetic field distribution is a symmetric cosine function ($A = B$), becomes a leaky mode because two radiating waves with $A\exp(+iKz)$ and $B\exp(-iKz)$ interfere constructively. Since the size of the band gap is given by

$$\Delta\Omega = |\mathrm{Re}(\Omega^a - \Omega^s)| = 2|h_2 - \mathrm{Im}(h_1)|/(Kh_0), \tag{8}$$

we interpret here the second stop band as being formed by the superposition of the two scattering processes due to the first and second Fourier harmonics of the periodic modulation of the dielectric function.

Since Eqs. (4) and (8) are valid for both TM and TE modes, the differing dynamics of the TM and TE band gaps can be seen by comparing the coupling coefficients for TM modes in Eqs. (5)–(7) with those for TE modes given by [29,30]

$$h_{0,\mathrm{TE}} = \Omega \int_{-\infty}^{\infty} \epsilon_0(x)\varphi_{\mathrm{TE}}(x)\varphi_{\mathrm{TE}}^*(x)dx, \tag{9}$$

$$h_{1,\mathrm{TE}} = i\frac{K^3\Omega^4\epsilon_1^2}{8}\int_{-d}^{0}\int_{-d}^{0} G_{\mathrm{TE}}(x,x')\varphi_{\mathrm{TE}}(x')\varphi_{\mathrm{TE}}^*(x)dx'dx, \tag{10}$$

$$h_{2,\mathrm{TE}} = \frac{K\Omega^2\epsilon_2}{4}\int_{-d}^{0}\varphi_{\mathrm{TE}}(x)\varphi_{\mathrm{TE}}^*(x)dx, \tag{11}$$

where $\varphi_{\mathrm{TE}}(x)$ characterizes the transverse TE mode profile and $G_{\mathrm{TE}}(x,x')$ denotes the Green's function for TE modes. For the symmetric lattice studied herein, $h_{0,\mathrm{TE}}$ and $\mathrm{Im}(h_{1,\mathrm{TE}})$ is positive irrespective of d and ρ, but $h_{2,\mathrm{TE}}$ is positive (negative) when $\rho<0.5$ ($\rho>0.5$) because $\epsilon_2 = (\Delta\epsilon/\pi)\sin(2\pi\rho)$ changes its sign when $\rho = 0.5$. When both ρ and $\Delta\epsilon$ are small, therefore, the TE-polarized symmetry-protected BIC appears at the upper band edge because the primary scattering process represented by $h_{2,\mathrm{TE}}$ dominates the secondary effect represented by $\mathrm{Im}(h_{1,\mathrm{TE}})$. But when ρ increases and approaches to 0.5, there is a chance for the secondary effect to overwhelm the primary process because the strength of $h_{2,\mathrm{TE}}$ gets weaker and becomes zero as ρ approaches to 0.5. With proper lattice parameters which give $h_{2,\mathrm{TE}} = \mathrm{Im}(h_{1,\mathrm{TE}})$, therefore, the second TE band gap closes near the $\rho = 0.5$. Before and after the band gap closure, the spectral location of the symmetry-protected BIC is reversed from the upper to lower band edge.

For the TM mode, the sign of $h_{0,\mathrm{TM}}$ in Eq. (5) is also positive irrespective of the lattice parameters d and ρ. Equation (6) indicates the sign of $h_{1,\mathrm{TM}}$ depends on d, but not on ρ. However, the sign of $h_{2,\mathrm{TM}}$ depends on both d and ρ. Comparing the coupling coefficients for TM modes in Eqs. (5)–(7) and those for TE mode in Eqs. (9)–(11), it is reasonable to infer that the second TM and TE band gaps exhibit different evolutions because the sign of $h_{1,\mathrm{TM}}$ and $h_{2,\mathrm{TM}}$ varies by d, while the sign of $h_{1,\mathrm{TE}}$ and $h_{2,\mathrm{TE}}$ is independent of d. Figures 4(a)–4(c) illustrate numerically calculated coupling coefficients, $h_{0,\mathrm{TM}}$, $\mathrm{Im}(h_{1,\mathrm{TM}})$, and $h_{2,\mathrm{TM}}$, respectively, as a function of d. As shown in Fig. 4(a), values of $h_{0,\mathrm{TM}}$ are positive irrespective of d. However, Figs. 4(b) and 4(c) demonstrate that the sign of $\mathrm{Im}(h_{1,\mathrm{TM}})$ and $h_{2,\mathrm{TM}}$ change as d increases. In contrast, the coupling coefficients for the TE mode illustrated in Figs. 4(d)–4(f) evidently show that the sign of $h_{0,\mathrm{TE}}$, $\mathrm{Im}(h_{1,\mathrm{TE}})$, and $h_{2,\mathrm{TE}}$, is always positive irrespective of d. Spectral location of a BIC edge and a leaky edge at the second TM band is determined by the primary scattering process represented by $h_{2,\mathrm{TM}}$; the auxiliary scattering process by $\mathrm{Im}(h_{1,\mathrm{TM}})$ is meaningful only when the strength of $h_{2,\mathrm{TM}}$ is substantially weak. We interpret herein that the coefficient $h_{2,\mathrm{TM}}$ is determined by the competition of two different terms $h_{2,\mathrm{TM1}} = (K/4)\int \xi_2(x)|\varphi_{\mathrm{TM}}(x)|^2 dx$ and $h_{2,\mathrm{TM2}} = -(1/4K)\int \xi_2(x)|d\varphi_{\mathrm{TM}}(x)/dx|^2 dx$. The coefficient $h_{2,\mathrm{TM1}}$ can be considered to represent the Bragg effect induced by the periodic modulation of the dielectric function in the z direction because $h_{2,\mathrm{TM1}}$ comes from the second derivative term $\partial[\xi(x,z)\cdot(\partial H_y/\partial z)]/\partial z$ in Eq. (1). Similarly, the coefficient $h_{2,\mathrm{TM2}}$ originates in the discontinuity of the dielectric constant at the surfaces of slab geometry in the x direction because $h_{2,\mathrm{TM2}}$ comes from the first derivative term $\partial[\xi(x,z)\cdot(\partial H_y/\partial x)]/\partial x$ in Eq. (1).

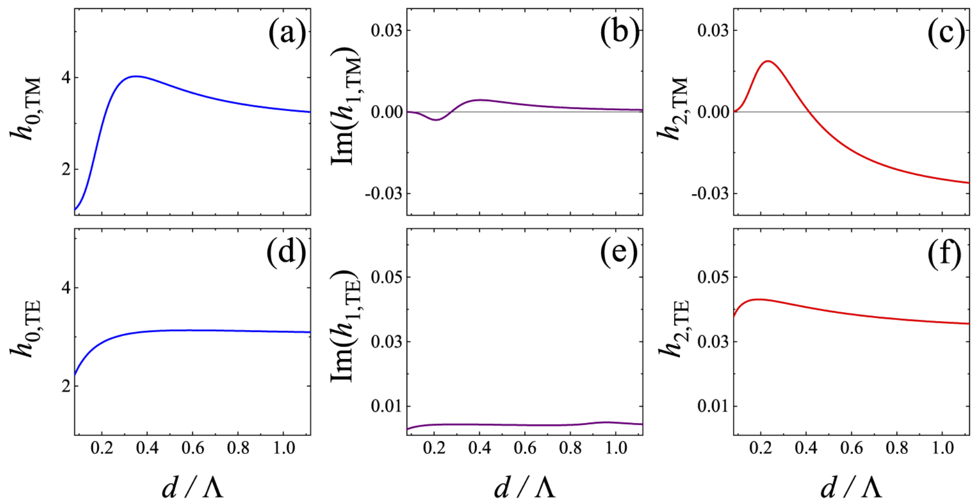

Fig. 4. Calculated coupling coefficients from the semianalytical dispersion model. (a) $h_{0,\mathrm{TM}}$, (b) $\mathrm{Im}(h_{1,\mathrm{TM}})$, (c) $h_{2,\mathrm{TM}}$, (d) $h_{0,\mathrm{TE}}$, (e) $\mathrm{Im}(h_{1,\mathrm{TE}})$, and (f) $h_{2,\mathrm{TE}}$ as a function of thickness. The second TM and TE band gaps exhibit different properties because the sign of $\mathrm{Im}(h_{1,\mathrm{TM}})$ and $h_{2,\mathrm{TM}}$ changes as d varies, while the sign of $\mathrm{Im}(h_{1,\mathrm{TE}})$ and $h_{2,\mathrm{TE}}$ is irrespective of d. Lattice parameters are the same as for Fig. 2.

When the thickness d is small so that the surface effect dominates the Bragg effect, as illustrated in Fig. 2(d), the spectral location of the TM-polarized BIC edge transfers from the upper to lower band as ρ varies from 0 to 1 because the sign of $h_{2,\mathrm{TM}}$ changes from positive to negative; this happens because $\xi_2 = (-\Delta\epsilon)/(\pi\epsilon_h\epsilon_l)\times\sin(2\pi\rho)$ changes its sign from negative to positive when $\rho = 0.5$. When d is thick enough so that the Bragg effect dominates the surface effect, in contrast, as illustrated in Fig. 2(f), the spectral location of the TM-polarized BIC edge transfers from the lower to the upper band because the sign of $h_{2,\mathrm{TM}}$ changes from negative to positive as ρ varies from 0 to 1. In the intermediate thickness state where the strength of the Bragg effect and surface effect are comparable to each other, as shown in Fig. 2(e), the second TM band gap is small and the gap can be closed two times by the variation of ρ.

5. Conclusion

In conclusion, we numerically and analytically investigate the band dynamics governing TM- and TE-polarized leaky modes in representative 1D photonic lattices. The leaky TM and TE band gaps open at the lattice Γ point due to the periodic dielectric-constant modulation. With clear understanding based on a semianalytical dispersion model, we show that both TM and TE band gaps are controlled by a primary first-order Bragg process due to the second Fourier harmonic and by an auxiliary second-order Bragg process due to the first Fourier harmonic. Major differences between the TM and TE band dynamics arise because the scattering process for the TM mode is

Optics EXPRESS

additionally governed by a surface effect due to the discontinuity of the dielectric constant at the interfaces of the photonic lattice. This surface effect is absent under TE polarization. When the lattice thickness d is small so that the surface effect dominates the Bragg effect, the spectral location of the TM-polarized BIC edge transfers from the upper to the lower band as ρ varies from 0 to 1. When d is large enough so that the Bragg effect dominates the surface effect, in contrast, the spectral location of the TM-polarized BIC edge transfers from the lower to the upper band. In the intermediate state where the Bragg effect and surface effect are comparable each other, the TM band gaps are very small due to the absence of major scattering processes. Our rigorous FEM simulations indicate that in the intermediate state, for the parametric set chosen for the research, the second TM band can exhibit a closed-band state two times, as ρ varies from 0 to 1. However, the spectral location of the TE-polarized BIC transfers only once from the upper to lower band edge irrespective of the thickness. The semianalytical model presented is key to successful interpretation of the results. It provides the explicit physical insight needed to understand the difference in the band dynamics associated with the TE and TM polarization states. The methodology revealed here for a relatively restricted parameter set can be widely applied for other cases of interest.

The semianalytical model presented is key to successful interpretation of the results. It provides the explicit physical insight needed to understand the difference in the band dynamics associated with the TE and TM polarization states. The methodology revealed here for a relatively restricted parameter set can be widely applied for other cases of interest. The impact of the work resides in its clear exposition of the fundamentals underlying the different properties of the TE and TM band dynamics. We believe this understanding can be transferred in large measure to the polarization band dynamics of 2D metamaterials lattices.

Funding

National Science Foundation (ECCS-1809143).

Disclosures

The authors declare that there are no conflicts of interest associated with this article.

References

1. A. Yariv and P. Yeh, *Optical Waves in Crystals* (Wiley, 1984).
2. J. D. Joannopoulos, R. D. Meade, and J. N. Winn, *Photonic Crystals: Molding the Flow of Light*, (Princeton University, 1995).
3. Y. Yang, C. Peng, Y. Liang, Z. Li, and S. Noda, "Three-dimensional coupled-wave theory for the guided mode resonance in photonic crystal slabs: TM-like polarization," Opt. Lett. **39**(15), 4498–4501 (2014).
4. S.-G. Lee and R. Magnusson, "Essential differences between TE and TM band gaps in periodic films at the first Bragg condition," Opt. Lett. **44**(19), 4658–4661 (2019).
5. W. Suh and S. Fan, "Mechanically switchable photonic crystal filter with either all-pass transmission or flat-top reflection characteristics," Opt. Lett. **28**(19), 1763–1765 (2003).
6. M. Niraula, J. W. Yoon, and R. Magnusson, "Single-layer optical bandpass filter technology," Opt. Lett. **40**(21), 5062–5065 (2015).
7. Y. H. Ko and R. Magnusson, "Wideband dielectric metamaterial reflectors: Mie scattering or leaky Bloch mode resonance?" Optica **5**(3), 289–294 (2018).
8. S.-G. Lee, S. H. Kim, K. J. Kim, and C. S. Kee, "Polarization-independent electromagnetically induced transparency-like transmission in coupled guided-mode resonance structures," Appl. Phys. Lett. **110**(11), 111106 (2017).
9. K. Yamada, K. J. Lee, Y. H. Ko, J. Inoue, K. Kintaka, S. Ura, and R. Magnusson, "Flat-top narrowband filters enabled by guided-mode resonance in two-level waveguides," Opt. Lett. **42**(20), 4127–4130 (2017).
10. K. Kawanishi, A. Shimatani, K. J. Lee, J. Inoue, S. Ura, and R. Magnusson, "Cross-stacking of guided-mode resonance gratings for polarization-independent flat-top filtering," Opt. Lett. **45**(2), 312–314 (2020).
11. H. S. Bark, G. J. Kim, and T.-I. Jeon, "Transmission characteristics of all-dielectric guided-mode resonance filter in the THz region," Sci. Rep. **8**(1), 13570 (2018).
12. J. M. Foley, S. M. Young, and J. D. Phillips, "Symmetry-protected mode coupling near normal incidence for narrow-band transmission filtering in a dielectric grating," Phys. Rev. B **89**(16), 165111 (2014).

Optics EXPRESS

13. Y. Plotnik, O. Peleg, F. Dreisow, M. Heinrich, S. Nolte, A. Szameit, and M. Segev, "Experimental observation of optical bound states in the continuum," Phys. Rev. Lett. **107**(18), 183901 (2011).
14. C. W. Hsu, B. Zhen, J. Lee, S.-L. Chua, S. G. Johnson, J. D. Joannopoulos, and M. Soljačić, "Observation of trapped light within the radiation continuum," Nature **499**(7457), 188–191 (2013).
15. Y.-X. Xiao, G. Ma, Z.-Q. Zhang, and C. T. Chan, "Topological subspace-induced bound state in the continuum," Phys. Rev. Lett. **118**(16), 166803 (2017).
16. K. Koshelev, A. Bogdanov, and Y. Kivshar, "Meta-optics and bound states in the continuum," Sci. Bull. **64**(12), 836–842 (2019).
17. E. N. Bulgakov and D. N. Maksimov, "Avoided crossings and bound states in the continuum in low-contrast dielectric gratings," Phys. Rev. A **98**(5), 053840 (2018).
18. M. Minkov, I. A. Williamson, M. Xiao, and S. Fan, "Zero-index bound states in the continuum," Phys. Rev. Lett. **121**(26), 263901 (2018).
19. L. Carletti, K. Koshelev, C. De Angelis, and Y. Kivshar, "Giant nonlinear response at the nanoscale driven by bound states in the continuum," Phys. Rev. Lett. **121**(3), 033903 (2018).
20. H. M. Doeleman, F. Monticone, W. den Hollander, A. Alú, and A. F. Koenderink, "Experimental observation of a polarization vortex at an optical bound state in the continuum," Nat. Photonics **12**(7), 397–401 (2018).
21. K. Fan, I. V. Shadrivov, and W. J. Padilla, "Dynamic bound states in the continuum," Optica **6**(2), 169–173 (2019).
22. Y. Yang, C. Peng, Y. Liang, Z. Li, and S. Noda, "Analytical perspective for bound states in the continuum in photonic crystal slabs," Phys. Rev. Lett. **113**(3), 037401 (2014).
23. K. Koshelev, S. Lepeshov, M. Liu, A. Bogdanov, and Y. Kivshar, "Asymmetric metasurfaces with high-Q resonances governed by bound states in the continuum," Phys. Rev. Lett. **121**(19), 193903 (2018).
24. X. Gao, B. Zhen, M. Soljačić, H. Chen, and C. W. Hsu, "Bound states in the continuum in low-contrast fiber Bragg gratings," ACS Photonics **6**(11), 2996–3002 (2019).
25. S. I. Azzam, V. M. Shalaev, A. Boltasseva, and A. V. Kildishev, "Formation of bound states in the continuum in hybrid plasmonic-photonic systems," Phys. Rev. Lett. **121**(25), 253901 (2018).
26. R. Gansch, S. Kalchmair, P. Genevet, T. Zederbauer, H. Detz, A. M. Andrews, W. Schrenk, F. Capasso, M. Loncar, and G. Strasser, "Measurement of bound states in the continuum by a detector embedded in a photonic crystal," Light: Sci. Appl. **5**(9), e16147 (2016).
27. S.-G. Lee, S. H. Kim, and C. S. Kee, "Bound states in the continuum (BIC) accompanied by avoided crossings in leaky-mode photonic lattices," Nanophotonics **9**(14), 4373–4380 (2020).
28. S.-G. Lee, S. H. Kim, and C. S. Kee, "Fourier-component-engineered metasurfaces support continuous bound states in the continuum and Dirac cone dispersions," arXiv preprint arXiv:2007.00352.
29. S.-G. Lee and R. Magnusson, "Band flips and bound-state transitions in leaky-mode photonic lattices," Phys. Rev. B **99**(4), 045304 (2019).
30. S.-G. Lee and R. Magnusson, "Band dynamics of leaky-mode photonic lattices," Opt. Express **27**(13), 18180–18189 (2019).
31. R. F. Kazarinov and C. H. Henry, "Second-order distributed feedback lasers with mode selection provided by first-order radiation loss," IEEE J. Quantum Electron. **21**(2), 144–150 (1985).
32. Y. Ding and R. Magnusson, "Band gaps and leaky-wave effects in resonant photonic-crystal waveguides," Opt. Express **15**(2), 680–694 (2007).
33. W. Streifer, D. R. Scifres, and R. D. Burnham, "TM-mode coupling coefficients in guided-wave distributed feedback lasers," IEEE J. Quantum Electron. **12**(2), 74–78 (1976).
34. K. Inoue and K. Ohtaka, *Photonic Crystals: Physics, Fabrication and Applications* (Springer-Verlag, Berlin Heidelberg, 2004).